UNIVERSIDAD COMPLUTENSE DE MADRID

FACULTAD DE CIENCIAS FÍSICAS

Máster en Astrofísica

TRABAJO DE FIN DE MÁSTER

Buscando polución por metales en una muestra de enanas blancas candidatas a exceso infrarrojo

Searching for metal pollution in a sample of White Dwarfs with candidate infrared excess

Ignacio Polo López

Supervisado por:

Markus Kissler-Patig (ESA/ESAC)

Amy Bonsor (University of Cambridge)

Siyi Xu (Gemini Observatory, NOIRLab)

Curso académico 2024-2025

Calificación: 8.5

Abstract

White dwarfs (WDs) are the remnant left after the death of intermediate-mass and FGK stars. They have become an important tool to measure the compositions of extrasolar planetary systems, as well as their formation and evolution, even after their host star death. This is possible thanks to the metal pollution of the White Dwarfs atmosphere, by which material from the planetary system can reach the star by different mechanisms and leaves metal spectral features in an atmosphere that should be composed of hydrogen only. Any heavier element will sink out of sight due to the enormous gravity. In the process of matter accretion, a dusty debris disc around the star can arise, causing an infrared excess on its spectrum. We conducted a spectroscopic analysis in a sample of 32 White Dwarfs candidate to display IR excess in order to identify metal pollution and search for candidates to display a dusty circumstellar disc. The objects were observed with the XSHOOTER spectrograph, installed at VLT. The seven most interesting objects were grouped in a subsample, where metal signatures were confirmed in three WDs, one of them (J0234-0406) highly polluted, with signs of Ca, Mg, Fe, Sc and V, as well as He. In the other two, only Ca was confirmed. The infrared excess was inspected for the seven stars in two catalogs of IR excess candidate WDs from the literature, making the three polluted objects interesting candidates to have a dusty disc. Finally, two WDs (J2257+0755 and J2316-5529) show Zeeman spectral line splitting that suggest their are magnetic.

Key words: White Dwarfs, pollution, metals, disc, circumstellar, accretion, infrared, excess, megnetism.

Resumen

Las enanas blancas son el remanente que queda tras la muerte de las estrellas de masa intermedia y de tipos FGK. Estos objetos se han convertido en una importante forma de medir la composición de sistemas planeatrios extrasolares, así como su formación y evolución incluso después de la muerte de la estrella anfitriona. Esto es posible gracias a la polución de la atmósfera de las enanas blancas por material procedente del sistema planetario, que puede alcanzar la estrella mediante distintos mecanismos y dejar firmas espectrales en una atmósfera que debería componerse únicamente de hidrógeno. Cualquier elemento más pesado se hundirá y dejará de ser visible debido a la intensa gravedad. En el proceso de acreción de material, un disco circumestelar de polvo se puede formar alrededor de la estrella, causando un exceso infrarrojo en su espectro. Hemos realizado el análisis espectroscópico de una muestra de 32 enanas blancas candidatas a presentar exceso en el infrarrojo para buscar contaminación en sus atmósferas y, con ello, candidatos a discos circumestelares. Los objetos fueron observados con el espectrógrafo XSHOOTER localizado en el VLT. Los siete objetos más interesantes fueron agrupados en una submuestra, en la que se confirmó la detección de metales en tres enanas, una de ellas (J0234-0406) altamente contaminada, con señales de Ca, Mg, Fe, Sc y V, además de He. En las otras dos sólo se confirmó la presencia de Ca. Para las siete estrellas se ha inspeccionado el exceso infrarrojo en dos catálogos de enanas candidatas a exceso obtenidos de la literatura, lo que convierte los tres objectos con polución en candidatos interesantes a la existencia de disco. Finalmente, dos enanas blancas (J2257+0755 y J2316-5529) muestran desdoblamineto Zeeman de líneas espectrales que sugiere su naturaleza magnética.

Palabras clave: Enanas blancas, polución, metales, disco, circumestelar, acreción, infrarrojo, exceso, magnetismo.

Contents

1 Introduction **4**
- 1.1 White Dwarfs . . . 4
- 1.2 The role of White Dwarfs in the study of exoplanets . . . 4
- 1.3 White Dwarfs classification . . . 6
- 1.4 This project . . . 6

2 Methodology **7**
- 2.1 The sample of White Dwarfs . . . 7
- 2.2 Observations . . . 7
- 2.3 Data reduction . . . 9

3 Analysis and results **12**
- 3.1 Lines identification . . . 12
- 3.2 Calculation of the line parameters . . . 13
- 3.3 Elements identified, defining the subsample . . . 14
- 3.4 List of the line properties . . . 15
- 3.5 The case of J2257+0755 and J2316-5529 . . . 16

4 Discussion **18**
- 4.1 Hydrogen and Helium Line Identification . . . 19
- 4.2 Metal Lines Detection . . . 20
- 4.3 Infrared Excess . . . 21
- 4.4 Magnetic White Dwarfs . . . 22

5 Conclusions and outlook **23**

6 Acknowledgments **24**

7 References **24**

1 Introduction

1.1 White Dwarfs

White dwarfs (hereafter WDs) are the remnant left after the death of intermediate-mass and FGK stars. The initial star underwent stellar evolution (burning Hydrogen and Helium to form a core of Carbon and Oxygen), but its intermediate mass did not allow it to generate enough gravitational energy to ignite Carbon and Oxygen: the nuclear fusion at its core stopped and the star remained in a collapsed state only supported by electron degeneracy pressure - with a mass insufficient for it to collapse further to become a neutron star or black hole. The physical properties of WDs are extreme and characterized by a very high density (about 10^6 times denser than the sun) leading to small diameter (1/100 of the solar radius and as small as Earth) and very high surface gravity ($\log g \approx 8 cm/s^2$). Although the core fusion has stopped, the residual heat of the former star leads to very high initial surface temperatures ($\sim$100,000 K) of the WD which cools very slowly - the temperature decreases exponentially with time, from $\sim$100,000 K to $\sim$1,000 K in a time interval similar to the Universe age (Bonsor et al. 2017). Thus, temperature is an indicator of the White Dwarf's age and one of its basic parameters, along with the surface gravity and, for our study, the atmosphere composition (e.g. Xu et al. 2021). Thanks to the abundant intermediate-mass stars and the sufficiently evolved state of the Universe, WDs are not only easy to find in the solar vicinity but they have also become very important and interesting objects in astrophysics.

Consequently, large surveys of WDs have been made to assemble large samples of these objects and to measure their physical properties. It is worth mentioning one such catalog created with data from ESA's Gaia mission (Gentile-Fusilo et al. 2021). This surveys led to understand WDs in multiple systems, i.e. in complex associations with other objects such as Brown dwarfs (Casewell et al. 2024 and Rebassa-Mansergas et al. 2022 as an example), which can be detected in infrared light.

One of the currently most promising fields of research associated with WDs, is the field of post-main-sequence planetary systems. In the last few decades it has been discovered the prevalence of planetary systems after their host star leaves the main sequence and even after it becomes a remnant. Given the large number of WDs and new methods to discover exoplanets, planetesimals and planetary debris around them, WDs can serve as an opportunity to understand the fate of planetary systems during the last stages of the star life and beyond them.

1.2 The role of White Dwarfs in the study of exoplanets

White Dwarfs allow us to study the general composition and hence understand the bulk density of planetary bodies around other stars. How is the composition of a planetary body measured? Due to the high surface gravity, the upper atmosphere of White dwarfs should be composed of hydrogen or helium only (Bédard 2024), with heavier elements sunk to the interior of the star (see Figure 1). However, around 30 % of known WDs show pollution of their surfaces by heavier elements (Bonsor et al. 2017). These heavier elements are the evidence for the existence of recent matter accretion onto the star. Indeed, the timescales of sinking heavy elements (from Myrs or timescales as short as days, Rogers et al. 2024) is much shorter than the cooling time of the star - polluted atmospheres testify of recent accretion.

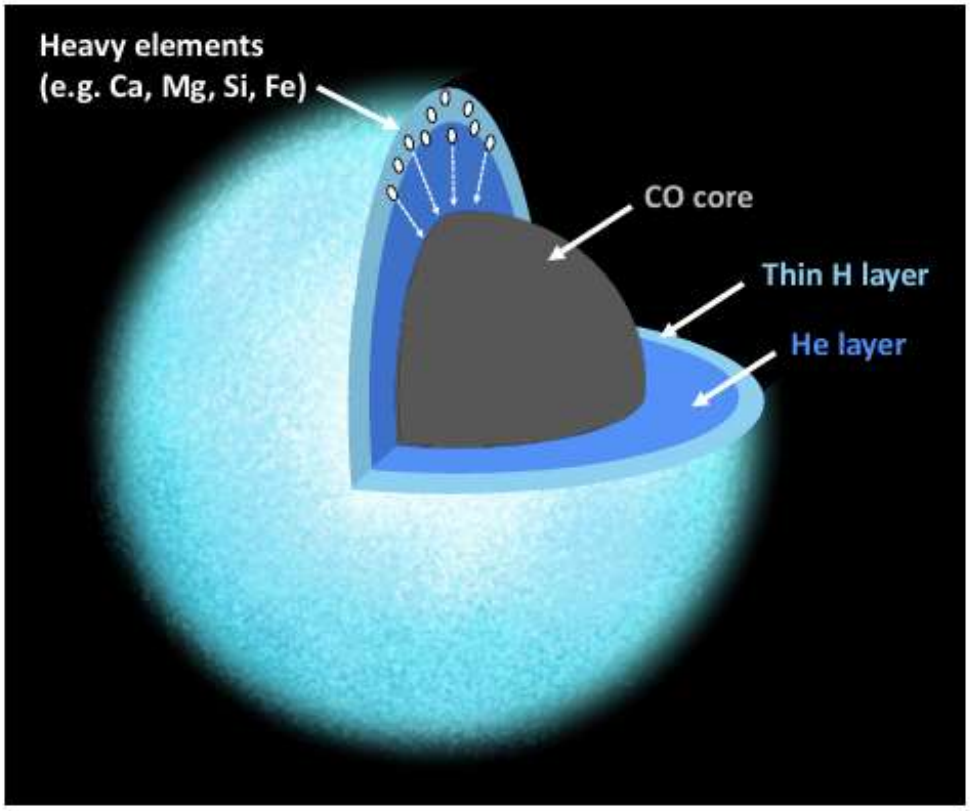

Figure 1: Schematic representation of the layered structure in a white dwarf. The surface is dominated by hydrogen while the heavier elements sink to the interior of the star - source: Xu et al. (2024).

Different mechanisms have been proposed to explain how the material from the planetary system can end up reaching the atmosphere of the WD, causing the photospheric pollution. When the star becomes a White dwarf there is a loss of mass from the outer layers, that are expelled to the inter-stellar medium (ISM). This causes major and minor planets to suffer changes in their orbits (Bonsor et al. 2017). Such changes can scatter smaller objects or even planetary bodies into the star. When these objects approach the WD, the tidal forces can disrupt and destroy them, enhancing the pollution. Changes in the system dynamics can also be favored by a companion of the WD, given that the mass loss amplifies possible gravitational secondary effects.

The pollution composition can give key information related to the planetary system architecture and hence its formation and evolution. The common composition measured so far from the material polluting WDs is similar to the one of Earth (Veras 2021). At least 18 elements have been found across the various cases - including Ca, Mg, Fe and Si (typical on Earth), and volatile elements such as C, S and N (Bonsor et al. 2017). The measured abundances can be a way to learn about the initial composition of the proto-planetary disk and further processes like migration of planets, which can mix material from different parts of the disk (Carter-Bond et al. 2012), and differentiation of an iron core inside larger bodies in the system. Through the measurement of abundance ratios, it is also possible to detect Fe-rich planetesimals in the WD atmosphere that were part of a dense planet core and planetesimals rich in mantle elements (Mg, Si) or crust elements (Al, Ca, Na, Ti) (Xu et al. 2021).

Another interesting aspect of WDs studies, is that these evolved stars can feature circumstel-

lar debris discs around them. These structures are formed by gas and/or dust and originate from disrupted bodies that enter the tidal radius of the WD and undergo tidal forces or collisions with other small bodies, which turn them into debris (Bonsor et al. 2017 and Veras 2021). Because of the proximity to the star, the heating of dust leads to an infrared excess in the Spectral Energy Distribution (SED) of the star. It has been found that 1-4 % of known WDs show an IR excess in their spectrum (Bonsor et al. 2017). Circumstellar gas has been detected in emission lines (Manser et al. 2020) as well as in absorption lines (Debes et al. 2012 and Xu et al. 2016). Recent studies show that among WDs with a dust disc detectable by infrared emission, 4 % are orbited by a gaseous disc detectable by gas emission, particularly through the Ca II 8600 A triplet emission (Manser et al. 2020). Some studies suggest that the presence of a circumstellar disk may be related to a certain stage in accretion onto the WD. Debris from objects can form an annulus of gas and dust, which can end up with sublimation and/or accretion by the star (Veras et al. 2020). In addition, there is evidence of ongoing accretion of objects by WDs. For example, in the case of WD 1145+017 (Xu et al. 2016), the star shows evidence of being orbited by several asteroid size objects, one of them suffering disintegration. This is observed in a burst of pollution, with 11 heavy elements detected, and possible gas streams from collisions between the disintegrating objects.

1.3 White Dwarfs classification

A common classification of White Dwarfs is according to their photospheric composition, which is inferred from their spectrum. The different categories, that depend on the spectral features of the optical spectrum (Bédard 2024, Xu et al. 2024) are: the DA White Dwarfs (the most important group), which show strong spectral lines of hydrogen; the DB White Dwarfs, which show lines of Helium; the DC White Dwarfs, that do not show strong lines, but rather show a continuum-dominated spectrum, with no remarkable lines; the DQ White Dwarfs that display Carbon signatures; while DZ White Dwarfs show presence of other metals in their atmosphere. The letter H indicates that the WD is magnetic. WDs can occasionally be classified in mixed groups - their names then list first the most important features followed by the less relevant ones. Some examples are DAZ, DBA or even DBAZ White Dwarfs. It is important to note that this classification can approximately indicate the photospheric composition of the star but is not always a clear hint of the dominant species. In order to find the dominant heavy elements in the atmosphere, high-resolution spectroscopy becomes essential.

1.4 This project

This above summary motivates the realization of this project, whose general objective is to characterize the pollution of WD atmospheres for stars that may feature a circumstellar disc. The studied WDs are part of a sample of 32 stars observed with the X-SHOOTER instrument on ESO's Very Large Telescope (European Southern Observatory 2021). These objects are part of a larger sample of 110 White Dwarfs that were selected as candidates to host infrared excess in their spectra (see Section 2). As mentioned above, this excess may be caused by a dust disc around the stars, which makes these objects interesting targets.

The main goal of this study is to inspect the spectra of the stars in our sample in search for hydrogen and helium lines, and potentially heavier elements. We will search for heavy elements such as Magnesium (Mg), Calcium (Ca), Silicon (Si) and Iron (Fe) detected previously in contaminated WDs. After that, the corresponding line widths will be measured. Knowing the basic parameters of

the star, the line widths allow us to measure abundances in the atmosphere of the star (Rogers et al. 2024). The procedure will shed light on whether an infrared excess confirmation in some of these objects would mean the presence of a dust disc or a companion star, such as a Brown dwarf.

This paper is structured as follows. In Section 2, we describe the observing program, the sample that we studied and the data reduction process. We list the main parameters of the white dwarfs in the sample (temperature, surface gravity and spectral classification). In Section 3, we present the main results of the spectra analysis. In Section 4, we discuss these results to finally expose, in Section 5, our conclusions from the study and the outlook for the future.

2 Methodology

2.1 The sample of White Dwarfs

The sample of 32 WDs studied in this work was obtained from 110 selected candidate objects to display IR excess (see Rebassa-Mansergas et al. 2019). These 110 stars come from the volume-limited sample of Jiménez-Esteban at al. 2018, which was built with objects at less than 100 pc using the second data release of Gaia satellite. The first selection criterion of Rebassa-Mansergas et al. was a color $G_{BP} - G_{RP} < 0,8$ to avoid the important contamination effects for cooler White Dwarfs. The second one was the existence of IR excess in the SED, which was built with VOSA tool from Virtual Observatory (Bayo et al. 2008) using a set of photometrical catalogs that cover the range from ultraviolet to the IR. The excess was detected thanks to IR photometry, comparing the observed flux to the expected one that comes from the SED fitting by VOSA for the WD contribution (not including the excess). 77 final candidates with near-IR and mid-IR photometry were selected. 33 additional objects with only mid-IR photometry were selected.

Data from the 32 white dwarfs is provided in Table 1. It contains the name of each white dwarf, the effective temperature and the surface gravity taken from the Gentile-Fusilo et al. 2021 catalog. It also lists the WD type from the Montreal White Dwarfs Database (Dufour et al. 2017), whether near-IR photometry was available and the corresponding observation program with X-SHOOTER (see next subsection). As previously mentioned, a confirmed excess shown by these objects can be caused by the presence of a circumstellar disc although this does not need always to be the cause. For example, J0007-1605 was discovered to be a triple system with two white dwarfs and one brown dwarf (Rebassa-Mansergas et al. 2022). Searching for metal lines, then, is important to detect pollution of the WD atmosphere that would hint at a debris disk surrounding the star as the origin of the excess.

2.2 Observations

The sample studied in this project was spectroscopically observed by the ESO Very Large Telescope (VLT) at Paranal Observatory. The 32 WDs were those from the original set of 110 objects which had an adequate declination for Paranal and were enough brilliant. Observations were divided in two programs, the first between October 2020 and December 2021 (Program 106.213V.001) and the second between October 2021 and February 2024 (Program 108.21WW.001). For the 32 objects, 24 come from the first program and 8 from the second one. In both programs the instrument used was the X-SHOOTER spectrograph (Vernet et al. 2011), mounted in the Cassegrain focus at Unit Telescope 3 (UT3) of VLT. This instrument is a cross-dispersed, echelle spectrograph which splits

WD name	Teff (K)	log g (cm/s^2)	WD type	Near-IR photometry?	Program
J0007-1605	11600± 200	7,878± 0,033	DA	Yes	First
J0016+0504	7300± 250	8,14± 0,11	DA	No	First
J0050-0326	24300± 900	9,04± 0,04	DA/DAH	Yes	First
J0205-7941	9360± 170	8,055± 0,047	DA	Yes	First
J0223-0459	10600± 200	8,139± 0,044	DA	Yes	First
J0234-0406	13100± 370	8,038± 0,035	DA	Yes	First
J0318-1300	7710± 260	7,95± 0,11	DA	No	First
J0329-4738	9340± 110	7,902± 0,033	DA	Yes	First
J0349-3031	6770± 160	7,78± 0,07	DA	No	First
J0412-4510	13900± 200	8,019± 0,018	DA	Yes	First
J0419-7303	17800± 400	7,925± 0,034	DA	Yes	First
J0501-1511	10810± 130	7,94± 0,03	DA	Yes	First
J0531-4558	10530± 160	7,967± 0,036	DA	Yes	First
J0602+0904	5960± 50	7,94± 0,03	DA	Yes	First
J0702+0003	12150± 160	8,087± 0,017	DA	Yes	First
J0734-6011	9960± 140	8,31± 0,03	DC	Yes	First
J0924-2423	8480± 120	7,993± 0,038	DA	Yes	First
J0933-1000	7840± 250	8,48± 0,08	DA	Yes	First
J1017-3236	7890± 80	7,86± 0,03	DA	Yes	First
J1154-3101	6240± 60	8,19± 0,03	DC	Yes	First
J2220-0041	8020± 190	8,03± 0,07	DA	Yes	First
J2233-3832	8170± 90	7,955± 0,032	DA	Yes	First
J2316-5529	9510± 120	8,25± 0,03	DA	Yes	First
J2340-3708	14600± 400	7,97± 0,04	DA	Yes	First
J0045-2503	6080± 260	8,41± 0,13	DA	No	Second
J0924+0521	5980± 160	7,99± 0,11	DAH	Yes	Second
J1240+0932	6490± 170	8,354± 0,074	DC	Yes	Second
J1518-1148	10350± 240	7,963± 0,057	DA	Yes	Second
J2106-1445	7500± 300	8,34± 0,11	DC	No	Second
J2153-2628	17600± 700	9,057± 0,038	DA	Yes	Second
J2233-0601	7680± 190	7,99± 0,08	DC	Yes	Second
J2257+0755	12700± 400	9,247± 0,034	DAH	Yes	Second

Table 1: White Dwarfs from the sample used in this project. We list the name, the effective temperature and surface gravity for each object, both taken from the Gentile-Fusilo et al. 2021 catalog, the WD type from the Montreal White Dwarf Data Base (Dufour et al. 2017), whether it is available near-IR photometry as stated in Rebassa-Mansergas et al. 2019 and the corresponding observation program at Paranal.

the light path in three different arms for ultraviolet-blue (UV-blue), visual-red and near infrared observations respectively. As it is seen in the scheme in Figure 2, light from the telescope enters the instrument shutter (in the top) and is guided to the arms thanks to a pair of dichroic mirrors. Each arm has its own spectrograph with an entrance slit that the incoming light passes through. Besides, the CCD at the infrared arm is equipped with a cryogenic unit to reduce the dark current effect from environment temperature, that can cause serious alterations in infrared observations.

A cross-dispersed echelle spectrograph is an astronomical instrument that uses a prism (for the cross-dispersion) combined with an echelle grating (for the high-resolution dispersion) to project many spectral orders and a broad wavelength range at high-spectral resolution on a detector. In practice, the slit spectrum is repeated in the focal plane several times, which are these spectral orders. The different orders can overlap, making it difficult to study the spectral features. A solution is to use a cross-disperser component (prism) to separate the different orders in the focal plane. The different orders can be stitched together to reconstruct a broad wavelength range over which to

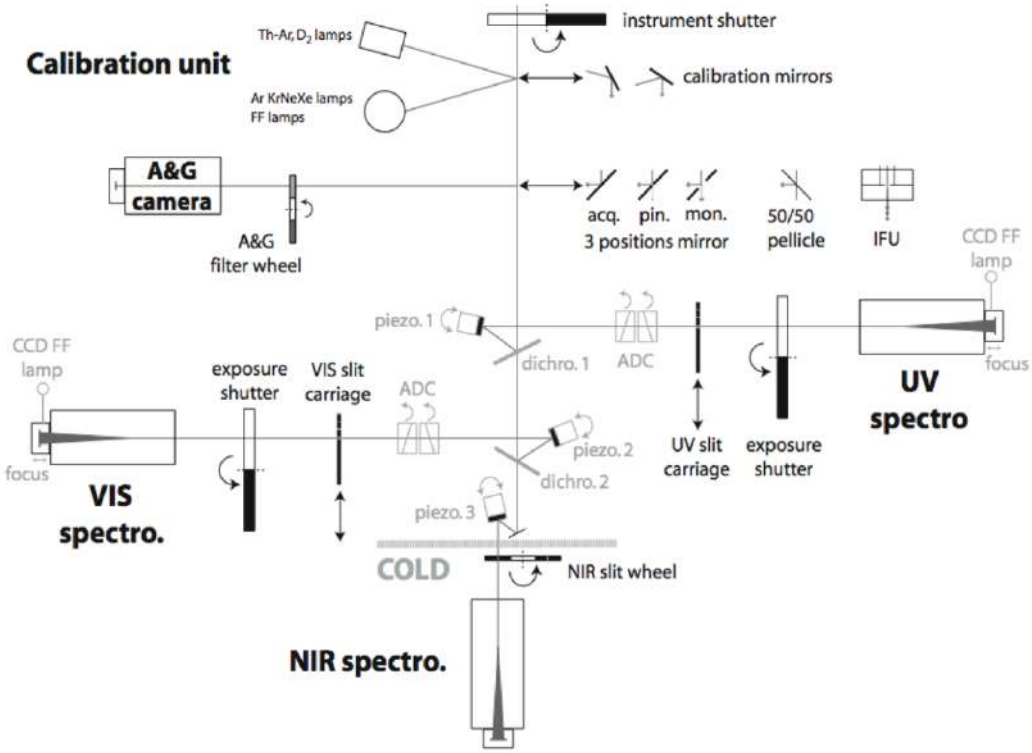

Figure 2: Schematic overview of the opto-mechanical design of X-SHOOTER - source: XSHOOTER User Manual (European Southern Observatory 2021).

examine the spectral characteristics of the observed star. The UV-blue arm of X-SHOOTER encompasses the wavelength range from 300 to 550 nm with 12 orders (European Southern Observatory 2021). The visual-red arm covers the range from 550 to 1000 nm in 14 orders. Finally the Near-IR arm covers from 1000 nm to 2500 nm in 16 orders. Thanks to this set up, XSHOOTER allows to span in a single observation the spectral range from UV to the K band in the near infrared (NIR). This instrument allows to study White Dwarfs spectra in a wide range of wavelengths, with an intermediate resolution (R = 3000-18000) that depends on the slit width and wavelength. Particularly, resolution takes the values R = 5400 for UV-blue light (with a 1" slit), R = 8900 for visual-red light (with a 0,9" slit) and R = 5600 for IR light (with a 0,9" slit).

2.3 Data reduction

The data reduction is the procedure by which the recorded data get cleaned from atmospheric, telescope and instrument signatures, and get calibrated in flux and wavelength. To perform the data reduction, a number of calibration and reference input data files are required next to the spectrum of the actual objetc of the study. For the reduction of the data in our sample, it was used the X-Shooter pipeline as implemented in the EsoReflex environment provided by ESO (European Southern Observatory 2024 and Freudling et al. 2013). This environment is designed to allow the easy reductions of data from the different astronomical facilities at Paranal and La Silla observatories. The reduction procedure allows to transform the photons counts in the different orders along the spectrum into a physical flux as a function of wavelength.

To calibrate the flux, the pipeline uses a catalogue of reference standard stars with known spectrum which allows to deduce the overall throughput of the instrument as a function of wavelength. To remove the Earth's atmospheric signature (telluric lines), we used telluric standards observed through the nights in which our data were obtained. These telluric standards are often DA White Dwarfs as these do not show any absorptions in the regions of the spectra where telluric absorption from the Earth atmosphere takes place. The wavelength calibration was achieved through the use of calibration lamps, which display a known pattern of spectral lines. This includes the use of Ar, Hg, Ne, halogen and ThAr lamps. These mentioned lamps are part of the calibration unit of the instrument, located at the entrance of the light from the telescope (see Fig. 2). Finally, the pipeline allowed us to subtract the main sky emission lines, as well as to correct for atmospheric extinction.

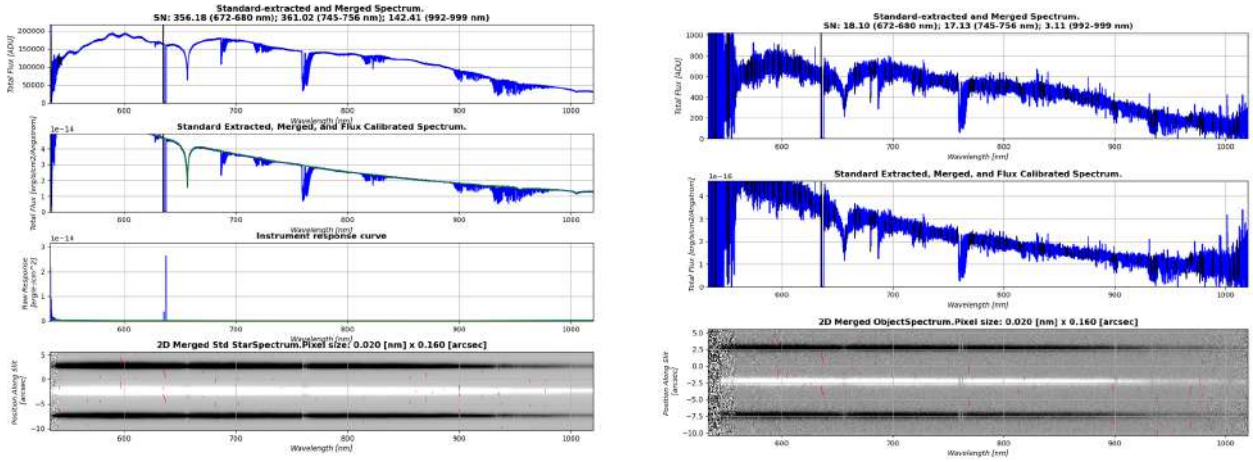

Figure 3: Results of the instrument response step (left) and the science reduction step (right) in X-Shooter pipeline for J1518-1148. In blue it is showed the flux of the object (in ADU or physical units; see Text) as a function of wavelength. The bottom panels show the two dimensions spectrum of the object, with the horizontal component as the wavelength and the vertical component (in degrees) as parallel with the slit width - The black lines encompass the ± sigma limit. If a sharp peak is not flagged with a black line, it could be caused by a cosmic ray impact rather than noise or artifacts from the setup. This is detected in the science reduction step.

In order to become familiar with the reduction task, we tested the X-Shooter pipeline with two of the WDs from the sample (J1518-1148 and J2257+0755), introducing all the necessary input data. The raw and calibration files were downloaded from the ESO data archive (European Southern Observatory 2025). The calibration input files included several arc-lamp frames (obtained illuminating one pinhole with a lamp) used to compute the instrumental throughput, calibrate wavelength and position of the spectrum in the 2D frames; bias frames used to inspect the read-out noise and fixed noise/defect pattern of the CCDs; dark frames taken to monitor the dark current; flat-field frames used to measure the response and efficiency of the detector at different spatial scales; and flux standards to calibrate the throughput. The pipeline also makes use of a set of static calibration data, which includes the model spectra of the reference standard stars. Once the pipeline is provided with all necessary calibration frames, the workflow is processed automatically. Throughout it, interactive windows appear that allow to check the intermediate results of the reduction and to change parameters (and, if needed, re-run certain parts of the pipeline). For this reduction procedure, the default values of the parameters were used.

The first interactive step corresponds to the instrument response. Figure 3 (left) shows an exam-

ple for the object J1518-1148. The upper panel shows the object spectrum in counts (or ADU) versus the wavelength in nm. Near 630 nm a sudden drop in flux is observed that is caused by a known fault of the instrument. The panel below shows the same spectrum in physical flux units ($erg/s/cm^2/\mathring{A}$) along with the spectrum of the catalogue reference standard (shown in green for comparison). The third panel plots the response of the instrument obtained from the standard observation (in green) and the last one plots, in two dimensions, the spectrum of the object in ADU, with the slit width in the direction of the vertical component (in arcsec). This step allows to check if the spectrum of the used reference star correctly fits the object data. The latter is important for the flux calibration to work properly.

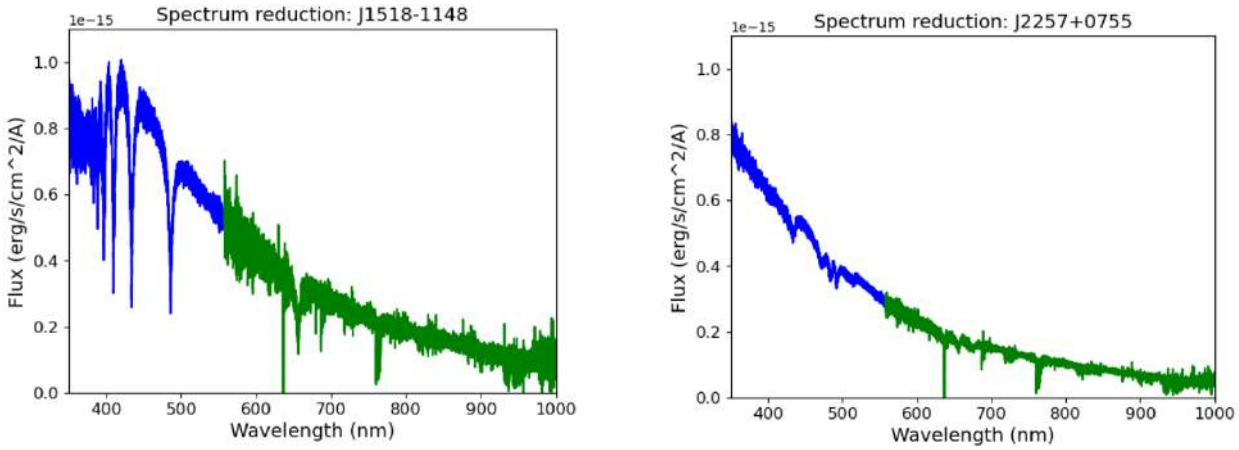

(a) WD: J1518-1148 (b) WD: J2257+0755

Figure 4: Results for both reduced WDs (J1518-1148 and J2257+0755). UV-blue and visual-red regimes are indicated in blue and green, respectively. It can be noted how the noisy peaks becomes more frequent in the visual arm. The infrared arm has not been included for clarity to show some spectral lines present in the spectra, such as the Balmer lines of hydrogen, easily noticeable for WD J1518-1148. The infrared arm features the highest noise level, which is due to thermal effects and absorption/emission by the Earth atmosphere. In fact, the use of a cryogenic unit in this arm pretends to reduce temperature effects.

Figure 3 (right) shows the next step that focuses on science reduction. The stellar spectrum is again plotted in counts (in one and two dimensions) and physical units but in this case with a lower signal-to-noise ratio than in the previous example. This window allows to monitor possible cosmic rays or artifacts that are registered by the detector or bad pixels. All these effects can introduce sharp peaks in the spectrum. It is important that all of the pixels with a sharp peak get flagged, this means that the peak is covered by the ± sigma limits, indicated by the black lines. If it is not the case, it means that the peak is very possibly caused by a cosmic ray rather than an artifact. After the workflow is completed, the calibrated spectrum for the objects J1518-1148 and J2257+0755 is obtained. A zoom for both cases is shown in Figure 4. The thermal effects make the infrared regime to have the biggest noise level and the UV-blue regime the smallest. Some features such as the Balmer hydrogen lines are seen, specially in J1518-1148.

3 Analysis and results

3.1 Lines identification

In the following, we describe how we search in the reduced spectra of the White Dwarfs sample for spectral features in their atmospheres. Specifically, the goal is to detect, or compute upper limits for, the elements H, He, Al, C, Ca, Fe, Li, Mg, O and Si. These atomic lines are predominantly in the optical-UV range, so that our analysis focuses on the data from UV-blue and visual-red arms of X-SHOOTER. Besides, the infrared regime is highly affected by the Earth atmosphere and important noise patterns, making detections less reliable.

To identify possible spectral signatures, we searched for a coincidence between absorption lines in the spectra and a series of reference wavelengths for the different elements that we took from Xu et al. (2024) and Klein et al. (2011) for metal lines and from the NIST Atomic Spectra Database (Ralchenko at al. (2005)) for H and He. An example of how this is done is shown in Figure 5 for the WD J1518-1148. The representation of the spectra has been performed with the library *Matplotlib* of Python. The solid vertical lines represent the location of the Balmer series of hydrogen, while the dashed lines represent the location of helium lines. This is to help distinguishing the lines series of the two elements. In addition, the first lines in the series are quite important as they are usually the deepest and most important ones.

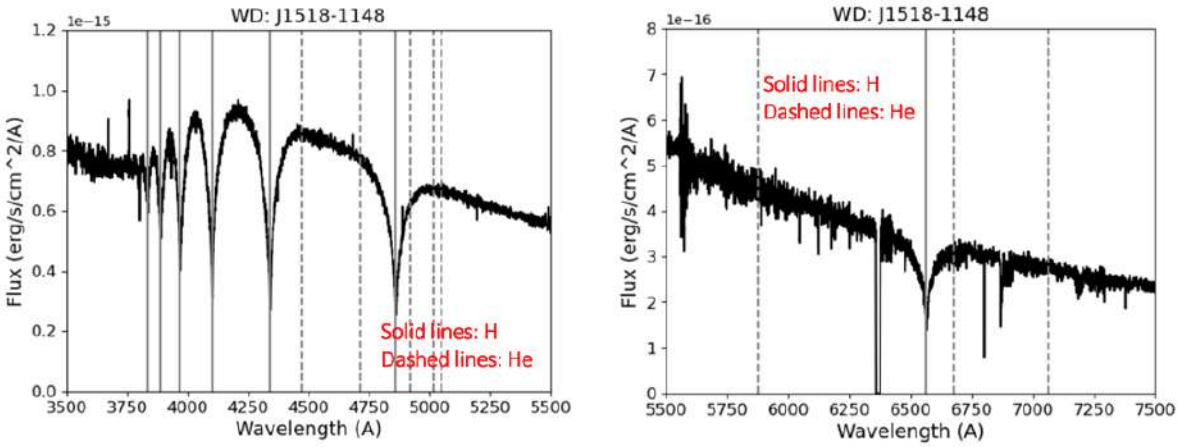

Figure 5: Example of lines identification for the White Dwarf J1518-1148 at two wavelength ranges. Reference lines are indicated for hydrogen (solid lines) and helium (dashed lines). It can be noted the clear signature of the Balmer series of hydrogen. Nontheless, helium lines are absent.

Our results indicate that the majority of the stars in the sample show hydrogen in their atmosphere, as expected and traced through the existence of the Balmer lines series in the spectrum. In some cases (see the spectrum of J1518-1148 in Fig. 5 as an example), Balmer lines are quite deep and defined. In other cases, however, they are less evident or even nonexistent. The last scenario is the case for the objects J0050-0326, J0734-6011, J1154-3101, J1240+0932, J2106-1445 and J2233-0601, which show a featureless spectrum. Helium is only confirmed in one star from our sample, the object J0234-0406. In other WDs, possible helium signatures were identified as false detections, maybe due to noise peaks or skylines badly subtracted in the reduction procedure. Finally, some metal lines, the object of our search, have been found, hinting at accreted material. A detailed description of

these is given in the Section 3.3.

3.2 Calculation of the line parameters

The next step is to obtain the basic parameters for the lines identified. This means fitting the line structure with a function of a given profile, which allows to calculate different line properties such as the central wavelength of the line, the equivalent width and the full width at half maximum (FWHM). The equivalent width is calculated as the line profile area below the continuum level (assuming absorption lines), divided by that continuum level. The FWHM is the width of the profile at the half of its maximum (emission) or minimum (absorption) flux value. We used a Voigt profile from the Python library *Scipy* for the fitting.

The FWHM is obtained from the following expression (Kielkopf 1973):

$$\Delta\lambda_{FWHM} = 0,5343 f_L + \sqrt{0,2169 f_L^2 + f_G^2} \tag{1}$$

In this expression, $f_L = 2 \times \gamma$ and $f_G = 2\sigma \times \sqrt{2 \times \log 2}$. The parameters γ and σ are two of the three parameters fixed in the Voigt profile fitting. The third one is the central wavelength of the line.

To fit the equivalent width of the lines, we first determined the continuum around the line to be fitted, i.e. the aspect the spectrum would have in absence of the corresponding absorption line. The continuum has been determined with a linear fit using the function *Polynomial.fit* from the library *Numpy* and considering a polynomial of degree one. The region to perform the linear fit has been chosen visually as wavelength ranges on both sides of the line that present a general linear trend between the flux and the wavelength.

After this step is completed, the fitted continuum $Cont(\lambda) = a + b \times \lambda$ is subtracted to the measured flux and the absolute value of the difference is divided by the continuum. This means we get a curve given by $y(\lambda) = 1 - Flux(\lambda)/Cont(\lambda)$. With the *curve_fit* function from the library *Scipy*, we have fitted this curve $y(\lambda)$ with a Voigt profile multiplied by an amplitude A ($A \times Voigt$). The Voigt profile is normalized, so assuming a line with a structure given by $A \times Voigt$ and the definition of the equivalent width, this width equals to the amplitude value A. The region in which the profile is fitted includes the central strip of the line and doesn't overlap with the region from which the continuum is determined.

To determine the error in the equivalent width, various factors are taken into consideration. First, the error in the amplitude that comes directly from the fitting process. Second, the noise in the measured flux, that is obtained from the reduction procedure with the X-Shooter pipeline. This means that each value of the flux has an associated measurement error. The last included contribution is related to the error in the continuum fit. The error in the slope and the ordered at the origin translates into an additional error in the y coordinates to be fitted. The three components of the error are added quadratically following the expression:

$$E_{final} = \sqrt{E_{fit}^2 + E_{flux}^2 + E_{cont}^2} \tag{2}$$

The first contribution is the error in the amplitude that comes directly from the profile fit ($E_{fit} = \Delta A$). The operation of the other two, from the measurement error and continuum uncertainty, is less straightforward. Both effects introduce an uncertainty in the y coordinate. The measurement error

has a value Δy_{flux}. In order to estimate the effect of the continuum fit, we used the uncertainty in the resulting line slope Δb, while the error at the origin Δa has been ignored. This last procedure is based on the assumption that the calculated line must pass through the Wavelength-flux point where the x coordinate takes the value λ_{medium}, which is the middle between the two furthermost wavelengths used to fit the continuum. In this way the error is calculated as:

$$\Delta y_{cont} = \frac{Flux(\lambda) \times |\Delta b \times (\lambda - \lambda_{medium})|}{Cont(\lambda)} \tag{3}$$

The equivalent width requires to compute the area between the profile and the continuum. Following the trapezoid rule, the errors contribution to the equivalent width are:

$$E_{flux} = \sqrt{\sum \frac{1}{4}(x_{i+1} - x_i)^2(\Delta y^2_{flux,i+1} + \Delta y^2_{flux,i})} \tag{4}$$

$$E_{cont} = \sqrt{\sum \frac{1}{4}(x_{i+1} - x_i)^2(\Delta y^2_{cont,i+1} + \Delta y^2_{cont,i})} \tag{5}$$

Finally, when only upper limits could be obtained, it was used a code developed and used by Rogers et al. 2024 to calculate them.

3.3 Elements identified, defining the subsample

As indicated by the results in Subsec.3.1, in the majority of the White Dwarfs the presence of hydrogen and absence of helium shows that hydrogen floats in the atmosphere and the WD displays only or mostly hydrogen lines. The only example with confirmed detection of helium lines is the case of J0234-0406, in which three helium lines can be identified (see Table 2 in Subsection 3.4).

Heavier elements in the atmosphere, as mentioned previously in this work, are not intrinsic to the White Dwarf, but trace material accreted onto the star from e.g. a disk of circumstellar dust and gas, or planet(esimal)s, etc (an idea pioneered by Jura 2003). The detection of these lines in our sample of WDs, candidates to display infrared excess (i.e. potential circumstellar material), was one of the principal motivators for this work.

The search for metal lines, however, has not yielded significant detections for most of the White Dwarfs in the entire sample. Following a visual inspection, the stars in which we saw or suspected to display signs of pollution were chosen as a subsample of objects to study in more detail. We selected all WDs in the spectroscopic sample which could show helium and/or metals pollution in their atmospheres based on the visual inspection of the spectra. These seven objects are the WDs J0234-0406, J0924+0521, J0933-1000, J1518-1148, J2220-0041, J2257+0755 and J2316-5529. Fortunately, NIR and MIR photometry was available for these WDs (see Tab.1). If only MIR photometry was available, it could be more difficult to the determine whether the potential excesses found by Rebassa-Mansergas et al. 2019 are well identified or not. Below, the detections for this stars are summarized briefly.

The object WD J0234-0406 is evidently the one that shows the highest pollution. There is a clear presence of hydrogen accompanied by weaker lines of helium. In the spectrum we also identified seven Ca lines, two lines of Fe, one line of Mg, one line of Sc and one line of V. Figure 6 shows an example of detection and fitting in this star for one line of Ca and the line of Mg. For WD J0924+0521, we detected some hydrogen lines. We also investigated possible helium lines, but

our analysis did not confirm these as a reliable detection. Similarly, in WD J0933-1000, possible signatures of Li and O were not confirmed as reliable detections. In particular, the detection of Li would have been surprising, as the line looks too deep and wide to be real. For the rejections of tentative detections, we relied (apart from other criteria) on the radial velocity of the WD (Doppler effect) as determined by the lines of the various elements (see next subsection). In WD J1518-1148, we detected the presence of hydrogen and one signature of Ca. For the WD J2220-0041, we detected hydrogen and Ca. A possible detection of helium at $5878,339\mathring{A}$ was rejected. According to the elements identified, the seven WDs type has been visually classified (see Sec.1) and indicated in Table 3.

In the last two White Dwarfs observed, we detected intriguing spectral structures due to line splitting, not visible in the other objects. As for abundances, in WD J2257+0755 we only detected hydrogen and rejected possible signals of He, Li, C, Ca, and Fe. Similarly, WD J2316-5529 was only confirmed to show hydrogen, with rejected detections of Li, Ca, Si and Al. The cases of J2257+0755 and J2316-5529 are further described in Subsection 3.5.

3.4 List of the line properties

For the subsample of the seven objects mentioned in the previous subsection, we calculated for each detected line the central wavelength, the equivalent width and the FWHM (see Table 2). We only considered the lines detected over the 3 sigma level in the equivalent width. The radial velocity derived from each line helped to identify possible spurious signatures. To obtain this velocity, we used the relativistic Doppler effect, which shifts the $\lambda_{emitted}$ value of a spectral line and changes it by a new $\lambda_{observed}$ value. Under the assumption that the star velocity with respect to us is much smaller than the speed of light, the WD velocity v can be derived from this expression, where c is the speed of light:

$$v = c \times (1 - \frac{\lambda_{emitted}}{\lambda_{observed}}) \tag{6}$$

In this equation a positive value of v means that the star is moving away from us, while a negative value means that it is approaching. Comparing the resulting velocity with the one derived from the strongest lines (such as the first Balmer lines of hydrogen) helps to detect false spectral features. We obtained the reference values $\lambda_{emitted}$ from Xu et al. 2024 and Klein et al. 2011 for metal lines and the NIST database for H and He. The value $\lambda_{observed}$ is the calculated central wavelength.

Along with these properties, we indicated in Table 2 the equivalent width upper limit (if no line was found) for the Mg $4481,1\mathring{A}$ line and the Ca K line $(3933,7\mathring{A})$, which is commonly observed when searching for pollution in WDs. In Tab. 3 we indicate which stars are candidates to infrared excess, as taken from Favieres et al. 2024 and the visual type identification for the seven objects based on the detected elements (see Subsection 1.3). It is also indicated the detection of IR excess from Murillo-Ojeda et al. 2025 (in prep.) and the assumed cause of this excess as noted by Rebassa-Mansergas et al. 2019 (from the SED visual inspection), which considered the seven stars as excess candidates.

Favieres et al. (2024) combined optical Gaia EDR3 and CatWISE infrared data to detected an excess in infrared around White Dwarfs. They defined two different infrared-excess criteria. The first one are the magnitude excesses in the infrared bands $W1$ and $W2$ (centered at 3,4 μm and 4,6 μm, respectively). The second one is the excess in the infrared $W1 - W2$ color. Objects showing an infrared excess in only one of these categories are defined as 'Only mag' and 'Only color', while

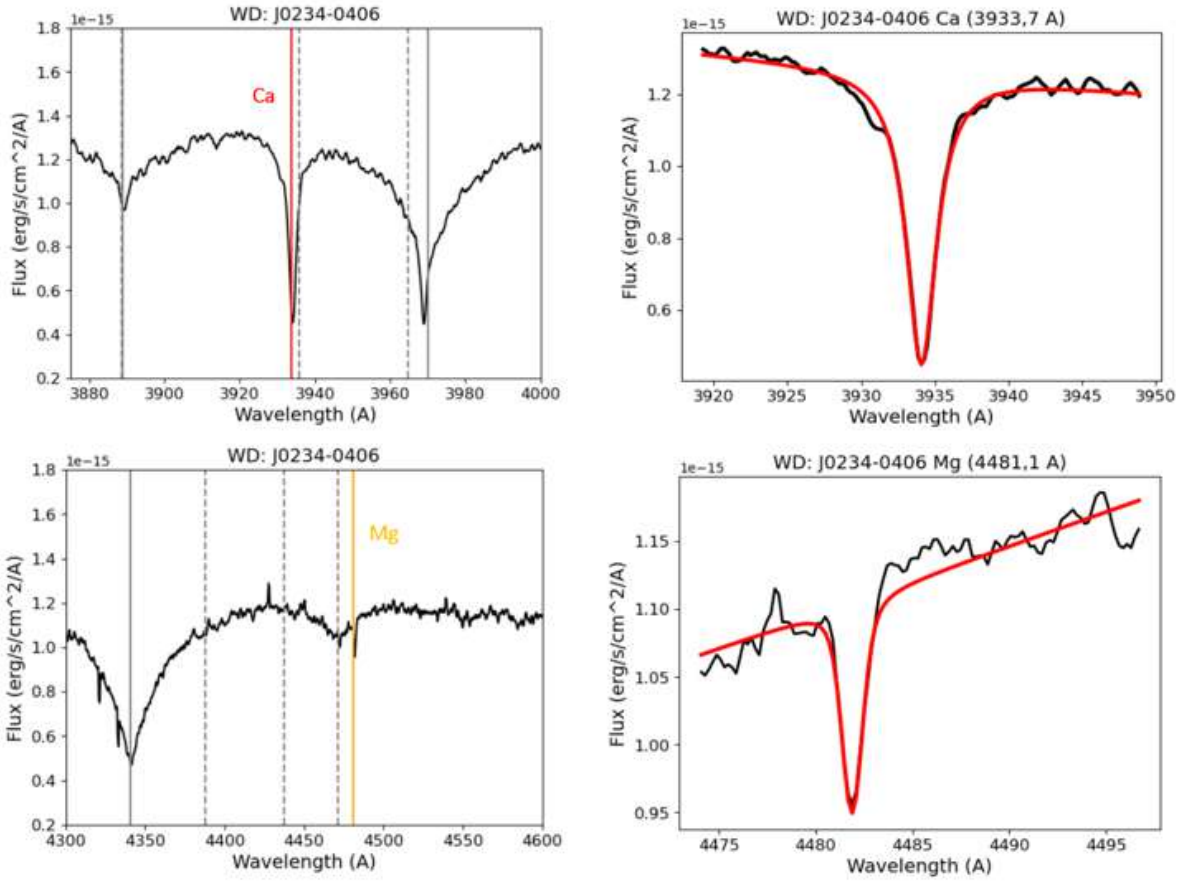

Figure 6: Example of the detection of two metal lines (Ca 3933.7$\AA$ and Mg 4481.1$\AA$) in the WD J0234-0406 (left column) along with the Voigt profiles (in red) fitted for each line (right column). The gray solid vertical lines indicate the position of the Balmer series of hydrogen, while the gray dashed vertical lines show the expected position of helium lines if they were present.

WDs satisfying both criteria are listed as 'Color+Mag'. As noted in Tab.3, only objects J0234-0406 and J1518-1148 show excess (in magnitude). The rest don't show excess while J0924+0521 was not classified by the authors. At the same time, nevertheless, Murillo-Ojeda et al. 2025 (in prep.) shows reliable excess in four objects and tentative in one of them. 'Tentative' means that the contamination is not rejected yet as a possible explanation to the excess.

3.5 The case of J2257+0755 and J2316-5529

As mentioned above, two objects (J2257+0755 and J2316-5529) show the presence of splitting spectral structures formed by three nearby peaks (Figure 7). This is especially noticeable near the first and second Balmer lines of hydrogen (around 6500$\AA$ and 4800$\AA$, respectively), with especially deep lines in the spectrum of J2316-5529. These line triplets are due to the splitting in Balmer lines of hydrogen, which was the only confirmed element in both WDs. The central peak was the one fitted to derive the line properties of the H line at 6562, 7$\AA$ in Table 2. It should be noted that the spectrum in J2316-5529 becomes very complex at wavelengths shorter than 4500$\AA$, while it remains flatter for J2257+0755.

WD	Line ($\AA$)	λ_{centr} ($\AA$)	FWHM ($\AA$)	Equivalent width ($\AA$)	v (km/s)
J0234-0406	H 6562,7	$6563,10 \pm 0,22$	$59,6 \pm 0,8$	$36,80 \pm 0,45$	18 ± 10
	He 7065,2	$7066,437 \pm 0,076$	$2,7 \pm 0,5$	$0,62 \pm 0,11$	$52,5 \pm 3,2$
	He 6678,2	$6679,36 \pm 0,05$	$1,36 \pm 0,12$	$1,07 \pm 0,16$	$52,1 \pm 2,3$
	He 5875,6	$5876,22 \pm 0,17$	$9,0 \pm 0,8$	$3,6 \pm 0,4$	32 ± 9
	Mg 4481,1	$4481,891 \pm 0,012$	$1,30 \pm 0,64$	$0,24 \pm 0,05$	$52,9 \pm 0,8$
	Ca 8662,1	$8664,04 \pm 0,12$	$3,8 \pm 2,2$	$1,20 \pm 0,32$	67 ± 4
	Ca 8542,1	$8543,1 \pm 0,1$	$4,2 \pm 0,6$	$1,98 \pm 0,16$	$35,1 \pm 3,5$
	Ca 8498,0	$8499,20 \pm 0,08$	$3,2 \pm 0,6$	$1,06 \pm 0,12$	$42,4 \pm 2,8$
	Ca 4226,7	$4226,82 \pm 0,05$	$2,4 \pm 0,6$	$0,18 \pm 0,04$	$8,5 \pm 3,6$
	Ca 3933,7	$3934,096 \pm 0,017$	$2,47 \pm 0,11$	$2,497 \pm 0,065$	$30,2 \pm 1,3$
	Ca 3736,9	$3737,47 \pm 0,04$	$1,1 \pm 0,4$	$0,290 \pm 0,044$	$45,8 \pm 3,2$
	Ca 3706,02	$3706,581 \pm 0,013$	$1,18 \pm 0,13$	$0,270 \pm 0,034$	$45,4 \pm 1,1$
	Sc 4320,7	$4321,13 \pm 0,04$	$0,82 \pm 0,35$	$0,145 \pm 0,038$	$27,6 \pm 2,8$
	V 4332,4	$4333,065 \pm 0,037$	$0,8 \pm 0,5$	$0,170 \pm 0,056$	$47,8 \pm 2,6$
	Fe 5018,4	$5016,52 \pm 0,09$	$6,6 \pm 1,2$	$0,83 \pm 0,06$	$112,4 \pm 5,4$
	Fe 5316,61	$5316,37 \pm 0,13$	$3,3 \pm 1,8$	$0,143 \pm 0,045$	14 ± 7
J0924+0521	H 6562,7	$6563,73 \pm 0,18$	18 ± 3	$6,64 \pm 0,43$	47 ± 8
	Mg 4481,1	-	-	$< 0,133$	-
	Ca 3933,7	-	-	$< 0,134$	-
J0933-1000	H 6562,7	$6564,45 \pm 0,15$	$16,0 \pm 0,5$	$12,80 \pm 0,38$	80 ± 7
	Mg 4481,1	-	-	$< 0,086$	-
	Ca 3933,7	-	-	$< 0,059$	-
J1518-1148	H 6562,7	$6564,12 \pm 0,24$	$56,14 \pm 0,74$	$37,3 \pm 0,5$	65 ± 11
	Mg 4481,1	-	-	$< 0,052$	-
	Ca 3933,7	$3934,160 \pm 0,033$	$1,05 \pm 0,11$	$0,273 \pm 0,033$	$35,1 \pm 2,5$
J2220-0041	H 6562,7	$6564,18 \pm 0,12$	$15,74 \pm 0,34$	$12,40 \pm 0,27$	$67,6 \pm 5,5$
	Mg 4481,1	-	-	$< 0,058$	-
	Ca 8542,1	$8544,936 \pm 0,013$	$1,06 \pm 0,22$	$0,300 \pm 0,066$	$99,57 \pm 0,46$
	Ca 3933,7	$3934,506 \pm 0,017$	$1,05 \pm 0,18$	$0,21 \pm 0,04$	$61,5 \pm 1,3$
J2257+0755	H 6562,7	$6558,35 \pm 0,17$	$29,7 \pm 0,9$	$8,86 \pm 0,18$	-199 ± 8
	Mg 4481,1	-	-	$< 0,063$	-
	Ca 3933,7	-	-	$< 0,029$	-
J2316-5529	H 6562,7	$6558,43 \pm 0,14$	$16,92 \pm 0,46$	$8,75 \pm 0,23$	$-195,3 \pm 6,4$
	Mg 4481,1	-	-	$< 0,048$	-
	Ca 3933,7	-	-	$< 0,064$	-

Table 2: Properties of the spectral features detected in the subsample of the seven WDs analyzed. The columns show for each WD: the reference wavelength of the line, the measured central wavelength, the full width at half maximum (FWHM), the equivalent width and the corresponding WD velocity (from the difference between the reference and the measured wavelength). Only lines detected over the 3 sigma level in the equivalent width were considered. If no line was detected for Ca $3933,7\AA$ and Mg $4481,1\AA$ it is indicated the upper limit for the equivalent width.

WD name	Visual clasif.	IR excess (MF 24)	IR excess*	Assumed excess cause (RM 19)
J0234-0406	DABZ	Only mag	Reliable	Disc
J0924+0521	DA	(not classified)	Reliable	Disc
J0933-1000	DA	No excess	(not classified)	-
J1518-1148	DAZ	Only mag	Tentative	Disc
J2220-0041	DAZ	No excess	Reliable	Disc
J2257+0755	DAH	No excess	Reliable	Disc
J2316-5529	DAH	No excess	No excess	Disc

Table 3: The second column indicates the WD type classification for the seven WDs in the subsample based on the spectral features found in this work. The third column shows the potential infrared excess classifications according to Favieres et al. 2024. 'Only mag' means that the excess was detected in the magnitude of the infrared bands $W1$ and $W2$ (centered at $3,4$ and $4,6\mu m$, respectively). The object J0924+0521 was not clasified by the authors of the study. IR excess* is the excess classification by Murillo-Ojeda et al. 2025 (in prep.), where J0933-1000 was not classified. 'Tentative' means that the contamination is not rejected yet as a possible explanation to the excess. The last column indicates the assumed cause of the IR excess as noted by Rebassa-Mansergas et al. 2019 (from the SED visual inspection).

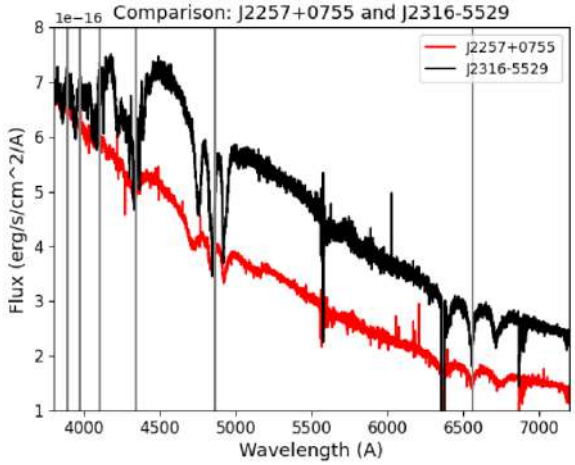

Figure 7: Comparison between the spectrum obtained for the objects J2257+0755 and J2316-5529. Reference hydrogen lines are indicated by the grey vertical lines. In both cases, three peaks structures are noticeable near the first and second Balmer lines of hydrogen (around $6500\mathring{A}$ and $4800\mathring{A}$, respectively). The spectrum from J2316-5529 shows clearly deeper lines and becomes very complex at wavelengths shorter than $4500\mathring{A}$.

4 Discussion

In this chapter, we discuss in more detail some of the findings of our work.

The identification of all spectral lines (around the expected wavelength as taken from Xu et al. 2024, Klein et al. 2011 and the NIST database) was based on their FWHM and equivalent width (EW) values, as well as the radial velocity derived from the shift in the central wavelength. We retained lines for which the FWHM and EW could be measured with errors significantly smaller than the measurement. In particular, for EW it was required a measure above the 3 sigma threshold. For the derived radial velocity, we discarded lines that returned inconsistent results (in sign and absolute

value) with respect to the values derived from the hydrogen lines (and clear He and Ca 3933.7$\mathring{A}$ lines, if present). All the lines retained as real features have an equivalent width larger than the measured upper limits for Ca 3933, 7$\mathring{A}$ and Mg 4481, 1$\mathring{A}$.

The Voigt profile used to derive the basic parameters of the lines was chosen to fit simultaneously the center of the line as well as the side wings. The Voigt profile is a convolution between a Gaussian profile which would underestimate the wings region, and a Lorentzian profile which would underestimate the central dip. In general, our fit matched well the observed data. In some cases, the Voigt profile underestimated the central peak but by no more than $10-20\%$ (see Figure 8 (left) for J0933-1000 as an example). Furthermore, the Voigt profile assumes a symmetric line structure. Although this is normally the case, in a few instances (such as the $H\alpha$ line in J2316-5529, see Fig. 8 (right)), the measured spectrum showed secondary bumps near the line or a multi-peaks structure. Overall, our values obtained for the equivalent width are consistent with previous studies of other WDs, as e.g. for HS 2253+8023 in Klein et al. (2011) or WD 1145+017 in Xu et al. (2016).

4.1 Hydrogen and Helium Line Identification

Our analysis of the spectra yielded the detection of hydrogen in most of the 32 White Dwarfs of the whole sample (and in all the objects of our subsample). This is consistent with the fact that the majority of the WDs belong to the type DA (see Sec.1). When present, the strength of the hydrogen lines can vary significantly from one star to another. In fact, the lines shape don't depend only in the hydrogen abundance, but also in other parameters such as the temperature or the surface gravity (Gray 2021), as them can affect the atoms excitation and velocities as well as the gas pressure.

As mentioned in Section 1, the surface of most WDs should be composed of hydrogen only, as the heavier elements (incl. helium) sink to the interior of the star. If an unperturbed sinking of heavy elements is assumed, a pure hydrogen atmosphere with prominent spectral features would be left and the absence of helium would become straightforward to explain. On the other hand, if none or little hydrogen is present with respect to helium, or the atmosphere is convective and gets mixed along the WD cooling sequence, helium can be detected in the atmosphere (e.g. see discussion in Cunningham et al. (2020)). The first case can take place when the WD loses the outer H layer (Bédard (2024)). We only confirmed the detection of helium in one object: J0234-0406. The spectrum of this WD shows both hydrogen and helium lines. This suggest the scenario of a mixed atmosphere with the two elements for that WD. The strength of the helium lines with respect to the hydrogen lines can serve as an indicator for the element abundances in the WD and its evolutionary history.

In six of the 32 objects of our total sample, we observed a featureless spectrum without any clear presence of hydrogen or helium lines. One of the flat spectrum stars, J0050-0326, is the hottest WD in the sample, with $T_{eff} = 24300 \pm 900$ (see Tab.1). At the same time, the star J1154-3101 is one of the coolest with $T_{eff} = 6240 \pm 60$. The absence of H and He lines could mean that nothing or little of these elements is present in the atmosphere, maybe due to outer layers lose, convective processes or other evolutionary mechanisms. However, it could also happen that one or both elements are present but don't show features above the detection level. This can occur with a too low temperature (H and He are not sufficiently excited at the right level to produce noticeable absorption lines in the optical) like J1154-3101 or a too high temperature (He and, especially, H atoms, are too excited and/or ionized to produce the lines) like J0050-0326 (Gray 2021).

4.2 Metal Lines Detection

The presence of metals was eventually confirmed in three of the WDs in our analyzed subsample, the White Dwarfs J0234-0406, J1518-1148 and J2220-0041. For the rest of cases, the equivalent width upper limits of Ca 3934$\mathring{A}$ and Mg 4481$\mathring{A}$ were calculated. In the three cases with detected pollution, at least calcium was detected (see Tab.2). This is not a surprise, as this element is the easiest to detect in the optical range when atmospheric pollution is present in a White Dwarf (Xu et al. 2024).

One of the WDs show an important level of pollution (J0234-0406), suggesting the existence of active accretion. This object shows the highest number of metal lines in the subsample. This includes common elements in the Earth core (Fe) and mantle (Mg) (Xu et al. 2021) as well as the refractory elements Ca, V and Sc. The detection of H and He hints at a strongly convective atmosphere with a mixture of H and He (see previous subsection). Ongoing work is studying this object in detail (Zuckerman et al. 2025 (in prep.)), reflecting the existence of a dozen of elements absorption features. Some of them are actually absorption lines from gas in a circumstellar disc, instead of photospheric signatures. This means that this WD is on a stage of accretion with a disc around it. Circumstellar lines show a broader profile due to the disc's velocity of rotation. Our spectral resolution, unfortunately, is not enough high to determine wether the lines found in this work originate from the disc or the photosphere. The parent body that causes the circumstellar and photospheric features is believed to be similar in composition to CI chondrites in the Solar System.

Another studied object is WD J2220-0041. The object J2220-0041, which shows the presence of calcium, was discovered to be a wide-separation (66 au) binary WD-Brown Dwarf binary system (Casewell et al. 2024, Steele et al. 2009), where the Brown Dwarf companion seems to be disrupting the orbits of planetesimals in the system, enhancing WD pollution. In Rebassa-Mansergas et al. 2019 the infrared excess cause of the system was wrongly assigned to a circumstellar disc (see Tab. 3).

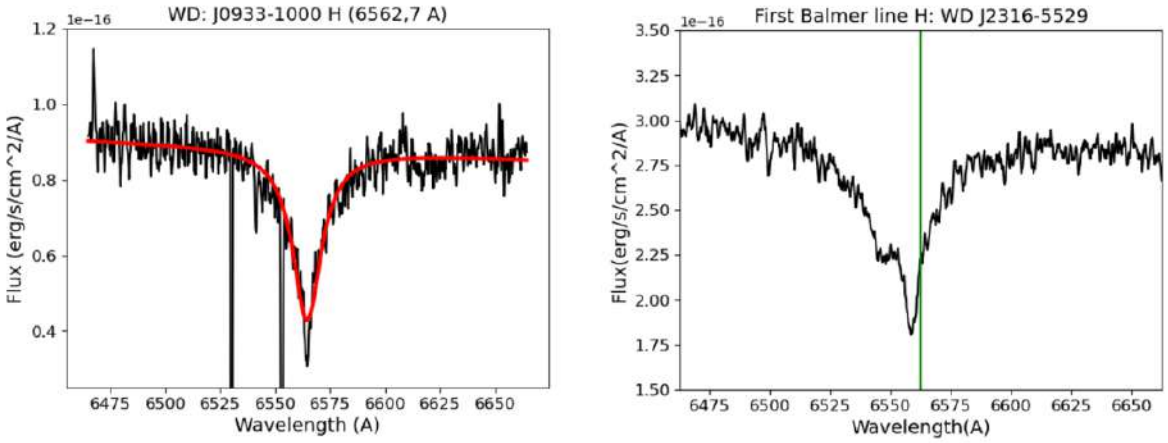

Figure 8: Left: example of a Voigt profile fitting (in red) of the $H\alpha$ line for the object J0933-1000. Right: asymmetric profile observed for the $H\alpha$ line from the object J2316-5529. In green it is indicated the reference wavelength of the line as obtained from the NIST database.

Once the equivalent widths of all the lines are measured, they can serve as a tool to derive the abundances in the WD atmosphere and accordingly of the accreted material. Although the equivalent width of an element increases with the abundance, the strongest spectral features not necessarily coincide with the dominant species (Xu et al. 2024), as other factors can affect the lines shape. To

derive the abundances, it is necessary to know the basic parameters of the atmosphere, the effective temperature and the surface gravity, accurately (Rogers et al. 2024). These parameters are required to build an atmosphere model from which to infer the element abundances. The goal is to obtain a synthetic spectrum that reproduces as better as possible the observed one. However, this procedure is beyond the scope of this work (which focuses on the line properties measurement) and should be carried out in future studies.

4.3 Infrared Excess

The infrared (IR) excess inspection as reported in Favieres et al. (2024) indicates excess in magnitude for two of the three polluted cases (J0234-0406 and J1518-1148). No excess above their threshold was found for the star J2220-0041. If a significant dusty debris disk were present around the star, we would expect it to display an excess of emission in the Spectral Energy Distribution (SED) at infrared wavelengths (see Sec.1). Accordingly, the absence of a strong excess in this case could suggest the lack of a significant debris disc around the White Dwarf. Note, however, that the existence of a debris disk may be only a stage in the accretion of material onto the WD. The dust could have been totally accreted by the star (Casewell at al. 2024), which would show pollution. It could also be the case that there is an optically thin dust disc, not detectable above the threshold chosen by the authors (Bonsor et al. 2017). In any case, Murillo-Ojeda et al. 2025 (in prep.) report reliable infrared excess in four objects (including J0234-0406 and J2220-0041) and tentative excess in J1518-1148, which supports the disc existence in these systems. In fact, circumstellar material has been detected for J0234-0406 (see previous subsection). On the other hand, J2220-0041 was confirmed to be a multiple system with a brown dwarf, which may be causing IR excess in the observed spectrum.

Murillo-Ojeda et al. 2025 (in prep.) uses a similar methodology to that used by Rebassa-Mansergas et al. 2019, but it used new data releases like Gaia early third data release or the CatWISE2020 infrared data release. This has helped to really increase the number of White Dwarfs with infrared excess within 100 pc. The lack of excess in Favieres et al.'s catalog for some of the objects may be due to the fact that the authors remained conservative in their identification to identify the high-confidence candidates. For example, they identified only the 59,6 % of the White Dwarfs with excess confirmed by Spitzer at that time (Favieres et al. 2024). Besides their final selection should not be taken as confirmed IR excess sources, because they were not able to exclude the 100 % of background contamination.

To sum up, we have identified a total of three polluted WDs (one of them highly polluted), all of them candidates to display excess as reported by Rebassa-Mansergas et al. 2019. As well, all of them display excess as noted by Murillo-Ojeda et al.'s catalog. This hints at the presence of a disc, already detected for J0234-0406. Although in the majority of the subsample WDs the IR excess source was assigned too be a disc (from the SED visual inspection) by Rebassa-Mansergas et al. 2019, further spectroscopic studies are needed to discard a ompanion origin, such as the case of J2220-0041. In any case, this study shows the importance of joining search of infrared excess in WDs, as well as pollution observations, to identify the existence of circumstellar discs, a quite interesting stage in the process of matter accretion onto WDs and a window to understand dynamics and composition of extrasolar systems.

4.4 Magnetic White Dwarfs

Two objects, J2257+0755 and J2316-5529 display 'triple-peaked' structures around lines in their spectra that are not visible in the other five stars. These structures are most clearly visible around the lines $H\alpha$ and $H\beta$ from the Balmer series of hydrogen. It is known that J2257+0755 is a magnetic White Dwarf with an atmopshere dominated by hydrogen (Williams et al. 2022), i.e. a DAH White Dwarf (see Table 1). The 'triple-peak' features that we identified are the result of the Zeeman splitting of the $H\alpha$ and $H\beta$ lines due to an extremely strong (Mega-Gauss) magnetic field. In the case of J2257+0755, the magnetic field strength has been measured to be $\approx 16.1MG$ (Külebi at al. 2009). Regarding the second star, it also shows very similar Zeeman line splitting as J2257+0755. Although J2316-5529 has not yet been studied in detail, these results indicate similar magnetic properties. Even though it is classified in the Montreal White Dwarf Data Base as DA (Dufour et al. 2017, see Tab.1), the machine learning tool available in the data base gives a DAH type, as expected from observations. The WD J0924+0521, in which only upper limits were obtained, is classified as DAH. Despite that, in this work it has been visually classified as DA (see Tab.3) because no signs of magnetic field have been found.

J2257+0755 and J2316-5529 have a mass of $1.29 \pm 0.01 M_{\odot}$ and $0.75 \pm 0.02 M_{\odot}$ respectively, based on a pure H atmosphere model (Gentile-Fusilo et al. 2021). The mass of J2257+0755 is around twice that of typical WDs (around $0,6 M_{\odot}$, Bonsor et al. 2017). This and other properties, such as a rotation period of $\approx 22.4 min$ found by Williams et al. 2022, suggest that this WD might be the remnant of the merger of two low-mass WDs rather than the single stellar evolution product of an intermediate-mass star. One of the signs of a WDs merger, along with rapid rotation or atmospheric composition, is the existence of a strong magnetic field like the one measured (Jewett at al. 2024). However, it should be noted that masses from Gentile Fusilo at al.'s catalog may not be totally confident, as they were obtained only from Gaia photometry.

In the other case, WD J2316-5529 does not seem as massive as J2257+0755, although above the normal values for WDs. At the beginning, it was suspected to display an important metal pollution. Possible signals of Ca, Si and Al were identified and the WD type was first assigned to be DAHZ, a magnetic and DA WD polluted with metals. Unfortunately, a comparison with the spectrum from the magnetic object SDSS J1014+3657 studied by Hardy et al. 2023 yielded a very similar behavior (Figure 9). The WD J1014+3657 was properly modeled in Hardy et al. 2023 assuming a magnetic star with a pure H atmosphere and a mean magnetic field strength of $7,01 MG$. This suggest that the metal features in J2316-5529 could actually be H lines split by the magnetic field, meaning it is a DAH White Dwarf. The line splitting makes the measurement and interpretation of abundances more difficult in J2316-5529. This is consistent with the absence of a dust disk and, accordingly, the absence of IR excess (see Tab.3). In Rebassa-Mansergas et al. 2019 non magnetic models were used to build the WDs SED. That could explain why the excess found for this object is not real. An atmospheric model including a strong magnetic field is needed to understand this object and the underlying physics.

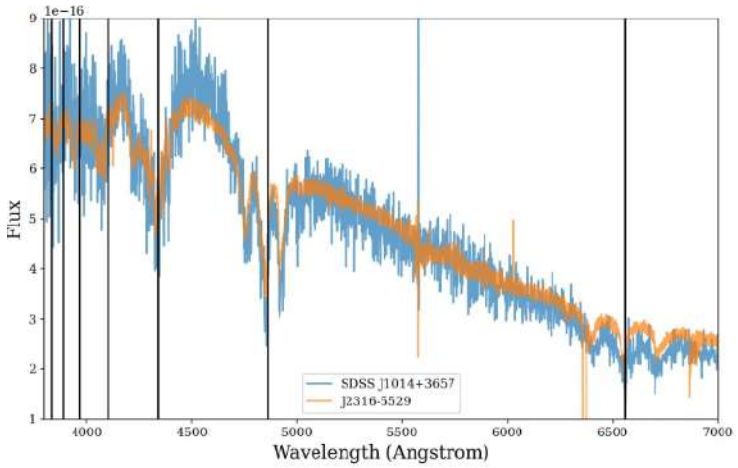

Figure 9: Comparison between the spectra from the WDs J2316-5529 from this work and SDSS J1014+3657 from Hardy el al. (2023). Reference hydrogen lines are indicated by the black vertical lines. It can be seen how the spectral features are very similar in both cases. The spectrum from SDSS J1014+3657 was modeled by Hardy et al. (2023) assuming a pure H atmosphere and a mean magnetic field strength of $7,01MG$.

5 Conclusions and outlook

A sample of 32 White Dwarfs, identified as showing infrared excess in their Spectral Energy Distribution (i.e. potentially surrounded by a dusty debris disk) by Rebassa-Mansergas et al. 2019, was followed-up spectroscopically with the X-SHOOTER instrument on ESO's Very Large Telescope, and inspected in search for metal pollution that would confirm that material gets accreted from a surrounding disk.

Most of the White Dwarfs show hydrogen lines as expected, although six of the 32 WDs show a featureless spectrum. These six stars could have undergone processes that eliminated the outer layers of H and He. Another possibility is that some of them are too cool (like J1154-3101) or too hot (like J0050-0326) to display lines of H and/or He even when these elements are present. This would mean that the elements are not excited enough or too excited and/or ionized, respectively.

We focused in this work on a subsample of seven WDs (J0234-0406, J0924+0521, J0933-1000, J1518-1148, J2220-0041, J2257+0755 and J2316-5529) that, based on a visual inspection of their spectra, were candidates for displaying signatures of He and/or metal lines. These seven stars all show hydrogen in their spectrum. Only one, J0234-0406 shows helium. Metals pollution was only confirmed in three cases J0234-0406, J1518-1148 and J2220-0041. The first one is highly polluted, with signatures of Fe and Mg (typical on Earth) as well as the refractory elements Ca, V and Sc. It is known to be accreting matter from a circumstellar disc. In the other two, we could only confirm the presence of Ca, which is the easiest metal to detect in the optical. One of them, J2220-0041, is a binary formed by a WD and a brown dwarf. For the remaining four stars in our sub-sample, equivalent width upper limits were derived for the lines Ca 3933.7$\mathring{A}$ and Mg 4481.1$\mathring{A}$. Line properties (central wavelength, FWHM and equivalent width) have been calculated for all detected lines. Furthermore, we calculated the WD radial velocity, as obtained from the Doppler shift between the central and reference wavelengths obtained from the literature.

Madurga Favieres at al. 2024 didn't observe IR excess in one of the three polluted objects,

J2220-0041, possibly because of their conservative detection threshold. In fact, Murillo-Ojeda at al. 2025 (in prep.) obtained excess detection for the three objects, suggesting the existence of a disc. However, further spectroscopic studies are needed to confirm a disc, as it can be the cause of the excess (the case of J0234-0406) or not (the case of J2220-0041).

Finally, the WDs J2257+0755 and J2316-5529 show interesting Hydrogen lines splitting, indicating strong magnetic fields in their atmposphere. We have classified them as DAH, magnetic WDs with a pure H atmosphere. J2257+0755 has been studied in previous works (Jewett at al. (2024), Williams et al. (2022), Hardy et al. (2023)) and is interpreted of being the product of a merger between two low-mass WDs. On the other hand, atmospheric and modeling of J2316-5529 is needed to better understand its properties.

This work intended to start a spectroscopic search for atmospheric pollution in a sample of WDs selected by their potential IR excess to look up for possible dusty debris-discs hosts. In particular, it is shown the utility to join the detection of infrared and metals pollution. It is a way to increase the number of known cases undergoing matter accretion from a circumstellar disc. The future will bring us many interesting results, given the new data releases of Gaia and the improved infrared catalogs that will come. Although this study is not complete enough to serve as a benchmark, it emphasizes the utility of WDs as a way to understand compositions and the fate of extrasolar systems in an era in which the search for life in other planets is becoming more and more significant.

6 Acknowledgments

I would like to acknowledge the supervision of Markus-Kissler Patig (ESA/ESAC), Amy Bonsor (University of Cambridge) and Siyi Xu (Gemini Observatory, NOIRLab) for the realization of this work and the paper preparation. I would also like to to acknowledge Alberto Rebassa-Mansergas (Universitat Politècnica de Catalunya) for all the spectroscopic data and Raquel Murillo-Ojeda for its help and the access to Murillo-Ojeda et al. 2025 (in prep.) catalog.

7 References

1) Bayo, A., Rodrigo, C., y Navascués, D. B., Solano, E., Gutiérrez, R., Morales-Calderón, M., & Allard, F. (2008). VOSA: virtual observatory SED analyzer-An application to the Collinder 69 open cluster. Astronomy & Astrophysics, 492(1), 277-287.
2) Bédard, A. (2024). The spectral evolution of white dwarfs: where do we stand?. Astrophysics and Space Science, 369(4), 43.
3) Bonsor, A., & Xu, S. (2017). White dwarf planetary systems: Insights regarding the fate of planetary systems. In Formation, Evolution, and Dynamics of Young Solar Systems (pp. 229-252). Cham: Springer International Publishing.
4) Carter-Bond, J. C., O'Brien, D. P., & Raymond, S. N. (2012). The compositional diversity of extrasolar terrestrial planets. II. Migration simulations. The Astrophysical Journal, 760(1), 44.
5) Casewell, S. L., Debes, J., Dupuy, T. J., Dufour, P., Bonsor, A., Rebassa-Mansergas, A., ... & Manjavacas, E. (2024). PHL 5038AB: is the brown dwarf causing pollution of its white dwarf host star?. Monthly Notices of the Royal Astronomical Society, 530(3), 3302-3309.
6) Cunningham, T., Tremblay, P. E., Gentile Fusillo, N. P., Hollands, M., & Cukanovaite, E. (2020). From hydrogen to helium: the spectral evolution of white dwarfs as evidence for convective mixing.

Monthly Notices of the Royal Astronomical Society, 492(3), 3540-3552.
7) Debes, J. H., Kilic, M., Faedi, F., Shkolnik, E. L., Lopez-Morales, M., Weinberger, A. J., ... & West, R. G. (2012). Detection of weak circumstellar gas around the DAZ white dwarf WD 1124-293: evidence for the accretion of multiple asteroids. The Astrophysical Journal, 754(1), 59.
8) Dufour, P., Blouin, S., Coutu, S., et al. 2017, in ASP Conf. Ser. 509, 20th European White Dwarf Workshop, ed. P. E. Tremblay, B. Gaensicke, & T. Marsh (San Francisco, CA: ASP)
9) European Southern Observatory.(2021, 5 of july).X-SHOOTER Instrument (instrument overview page).https://www.eso.org/sci/facilities/paranal/instruments/xshooter.html
10) European Southern Observatory. (2024, 12 of march). Science Software.https://www.eso.org/sci/software.html
11) European Southern Observatory. (2025, 29 of august). Archive Home.https://archive.eso.org/cms.html
12) Favieres, C. M., Kissler-Patig, M., Xu, S., & Bonsor, A. (2024). A sample of 554 white dwarfs showing infrared excess from Gaia EDR3 and CatWISE catalogs. Astronomy & Astrophysics, 688, A168.
13) Freudling, W., Romaniello, M., Bramich, D. M., Ballester, P., Forchi, V., García-Dabló, C. E., ... & Neeser, M. J. (2013). Automated data reduction workflows for astronomy-the eso reflex environment. Astronomy & Astrophysics, 559, A96.
14) Gentile Fusillo, N. P., Tremblay, P. E., Cukanovaite, E., Vorontseva, A., Lallement, R., Hollands, M., ... & Jordan, S. (2021). A catalogue of white dwarfs in Gaia EDR3. Monthly Notices of the Royal Astronomical Society, 508(3), 3877-3896.
15) Gray, D. F. (2021). The observation and analysis of stellar photospheres. Cambridge university press.
16) Hardy, F., Dufour, P., & Jordan, S. (2023). Spectrophotometric analysis of magnetic white dwarf–I. Hydrogen-rich compositions. Monthly Notices of the Royal Astronomical Society, 520(4), 6111-6134.
17) Jewett, G., Kilic, M., Bergeron, P., Moss, A., Blouin, S., Brown, W. R., ... & Agüeros, M. A. (2024). Massive White Dwarfs in the 100 pc Sample: Magnetism, Rotation, Pulsations, and the Merger Fraction. The Astrophysical Journal, 974(1), 12.
18) Jiménez-Esteban, F. M., Torres, S., Rebassa-Mansergas, A., Skorobogatov, G., Solano, E., Cantero, C., & Rodrigo, C. (2018). A white dwarf catalogue from Gaia-DR2 and the Virtual Observatory. Monthly Notices of the Royal Astronomical Society, 480(4), 4505-4518.
19) Jura, M. (2003). A tidally disrupted asteroid around the white dwarf G29-38. The Astrophysical Journal, 584(2), L91.
20) Kielkopf, J. F. (1973). New approximation to the Voigt function with applications to spectral-line profile analysis. Journal of the optical society of america, 63(8), 987-995.
21) Klein, B., Jura, M., Koester, D., & Zuckerman, B. (2011). Rocky extrasolar planetary compositions derived from externally polluted white dwarfs. The Astrophysical Journal, 741(1), 64.
22) Külebi, B., Jordan, S., Euchner, F., Gänsicke, B. T., & Hirsch, H. (2009). Analysis of hydrogen-rich magnetic white dwarfs detected in the Sloan Digital Sky Survey. Astronomy & Astrophysics, 506(3), 1341-1350.
23) Manser, C. J., Gänsicke, B. T., Gentile Fusillo, N. P., Ashley, R., Breedt, E., Hollands, M., ... & Pelisoli, I. (2020). The frequency of gaseous debris discs around white dwarfs. Monthly Notices of the Royal Astronomical Society, 493(2), 2127-2139.
24) Payne, M. J., Veras, D., Holman, M. J., & Gänsicke, B. T. (2016). Liberating exomoons in white dwarf planetary systems. Monthly Notices of the Royal Astronomical Society, 457(1), 217-231.
25) Ralchenko, Y. (2005). NIST atomic spectra database. Memorie della Società Astronomica Italiana Supplement, v. 8, p. 96 (2005), 8, 96.

26) Rebassa-Mansergas, A., Solano, E., Xu, S., Rodrigo, C., Jiménez-Esteban, F. M., & Torres, S. (2019). Infrared-excess white dwarfs in the Gaia 100 pc sample. Monthly Notices of the Royal Astronomical Society, 489(3), 3990-4000.
27) Rebassa-Mansergas, A., Xu, S., Raddi, R., Pala, A. F., Solano, E., Torres, S., ... & Cruz, P. (2022). Gaia 0007–1605: An Old Triple System with an Inner Brown Dwarf–White Dwarf Binary and an Outer White Dwarf Companion. The Astrophysical Journal Letters, 927(2), L31.
28) Rogers, L. K., Bonsor, A., Xu, S., Dufour, P., Klein, B. L., Buchan, A., ... & Zuckerman, B. (2024). Seven white dwarfs with circumstellar gas discs I: white dwarf parameters and accreted planetary abundances. Monthly Notices of the Royal Astronomical Society, 527(3), 6038-6054.
29) Steele, P. R., Burleigh, M. R., Farihi, J., Gänsicke, B. T., Jameson, R. F., Dobbie, P. D., & Barstow, M. A. (2009). PHL 5038: a spatially resolved white dwarf brown dwarf binary. Astronomy & Astrophysics, 500(3), 1207-1210.
30) Veras, D., & Heng, K. (2020). The lifetimes of planetary debris discs around white dwarfs. Monthly Notices of the Royal Astronomical Society, 496(2), 2292-2308.
31) Veras, D. (2021). Planetary systems around white dwarfs. arXiv preprint arXiv:2106.06550.
32) Vernet, J., Dekker, H., d'Odorico, S., Kaper, L., Kjaergaard, P., Hammer, F., ... & Zacchei, A. (2011). X-shooter, the new wide band intermediate resolution spectrograph at the ESO Very Large Telescope. Astronomy & Astrophysics, 536, A105.
33) Williams, K. A., Hermes, J. J., & Vanderbosch, Z. P. (2022). The Rapid Rotation of the Strongly Magnetic Ultramassive White Dwarf EGGR 156. The Astronomical Journal, 164(4), 131.
34) Xu, S., Jura, M., Dufour, P., & Zuckerman, B. (2016). Evidence for gas from a disintegrating extrasolar asteroid. The Astrophysical Journal Letters, 816(2), L22.
35) Xu, S., & Bonsor, A. (2021). Exogeology from polluted white dwarfs. Elements: An International Magazine of Mineralogy, Geochemistry, and Petrology, 17(4), 241-244.
36) Xu, S., Rogers, L. K., & Blouin, S. (2024). The chemistry of extra-solar materials from white dwarf planetary systems. Reviews in Mineralogy and Geochemistry, 90(1), 171-197.